Behavioral/Cognitive

Pulvinar Response Profiles and Connectivity Patterns to Object Domains

Haojie Wen,[1,2,3] Yingchao Song,[4] Meng Liang,[4] Peng Zhang,[5] Xiaoying Wang,[1,2,3] and Yanchao Bi[1,2,3,6]

[1]State Key Laboratory of Cognitive Neuroscience and Learning, Beijing Normal University, Beijing, 100875, China, [2]IDG/McGovern Institute for Brain Research, Beijing Normal University, Beijing, 100875, China, [3]Beijing Key Laboratory of Brain Imaging and Connectomics, Beijing Normal University, Beijing, 100875, China, [4]School of Medical Technology, School of Medical Imaging, Tianjin Key Laboratory of Functional Imaging, Tianjin Medical University, Tianjin, 300070, China, [5]State Key Laboratory of Brain and Cognitive Science, Beijing MRI Center for Brain Research, Institute of Biophysics, Chinese Academy of Sciences, Beijing, 100101, China, and [6]Chinese Institute for Brain Research, Beijing, 102206, China

Distributed cortical regions show differential responses to visual objects belonging to different domains varying by animacy (e.g., animals vs tools), yet it remains unclear whether this is an organization principle also applying to the subcortical structures. Combining multiple fMRI activation experiments (two main experiments and six validation datasets; 12 females and 9 males in the main Experiment 1; 10 females and 10 males in the main Experiment 2), resting-state functional connectivity, and task-based dynamic causal modeling analysis in human subjects, we found that visual processing of images of animals and tools elicited different patterns of response in the pulvinar, with robust left lateralization for tools, and distinct, bilateral (with rightward tendency) clusters for animals. Such domain-preferring activity distribution in the pulvinar was associated with the magnitude with which the voxels were intrinsically connected with the corresponding domain-preferring regions in the cortex. The pulvinar-to-right-amygdala path showed a one-way shortcut supporting the perception of animals, and the modulation connection from pulvinar to parietal showed an advantage to the perception of tools. These results incorporate the subcortical regions into the object processing network and highlight that domain organization appears to be an overarching principle across various processing stages in the brain.

Key words: animal domain network; domain selectivity; pulvinar; subcortical; tool domain network

---

Significance Statement

Viewing objects belonging to different domains elicited different cortical regions, but whether the domain organization applied to the subcortical structures (e.g., pulvinar) was unknown. Multiple fMRI activation experiments revealed that object pictures belonging to different domains elicited differential patterns of response in the pulvinar, with robust left lateralization for tool pictures, and distinct, bilateral (with rightward tendency) clusters for animals. Combining the resting-state functional connectivity and dynamic causal modeling analysis on task-based fMRI data, we found domain-preferring activity distribution in the pulvinar aligned with that in cortical regions. These results highlight the need for coherent visual theories that explain the mechanisms underlying the domain organization across various processing stages.

Introduction

One of the broad principles of visual object processing in the human cortex is domain structure. Viewing several domains of objects, including animals, small manipulable objects (tools), and large nonmanipulable objects, has been found to elicit different patterns of response in distributed cortical regions, including and beyond the ventral temporal cortex, which has been explained by their association with evolutionary-salient functions, such as fight-or-flight (animals) or manipulation (tools) (He et al., 2013; Konkle and Caramazza, 2013; Garcea and Buxbaum, 2019; Schone et al., 2021; Wen et al., 2022; for review, see Bi et al., 2016; Peelen and Downing, 2017). Viewing tools elicits activation in a left-lateralized cortical network, including the left lateral occipitotemporal cortex, the inferior and superior parietal lobule, and the medial fusiform gyrus, which have been

proposed to process various properties of tools that support its shape, use, and function (Brandi et al., 2014; Fabbri et al., 2016; Chen et al., 2018; Wang et al., 2018). Viewing animals elicits activation in the bilateral/right lateral fusiform (and amygdala), which is assumed to reflect visual and emotional properties associated with animals (Mormann et al., 2011; J. Yang et al., 2012; Bi et al., 2016). While the functionality of these domain-preferring cortical regions has been extensively studied, the potential roles of subcortical regions that are richly connected with the cortex remain poorly understood.

Among the visual-related subcortical areas (Saalmann and Kastner, 2011; Bridge et al., 2016; Fiebelkorn and Kastner, 2019; Jaramillo et al., 2019; Guedj and Vuilleumier, 2020), pulvinar, the largest nucleus in the primate thalamus, has shown particularly intriguing selectivity patterns for certain types of visual stimuli. Functional imaging, lesion, and animal evidence have indicated that the pulvinar is sensitive to salient visual objects, including threatening faces (Ward et al., 2007; Koizumi et al., 2019; McFadyen et al., 2019, 2020) and animals (i.e., snake) (Le et al., 2013, 2016). Sensitivity to nonthreatening faces has also been reported in the pulvinar (Nguyen et al., 2016; McFadyen et al., 2017; Arcaro et al., 2018). Based on indirect evidence, it has been speculated that the pulvinar may also be involved in tool processing. Pulvinar lesion leads to deficits in reaching and grasp (Wilke et al., 2018), which were closely related to tool use. When V1 is blocked, dorsal cortical areas still showed robust activation to images of tools, which has been assumed to be achieved through direct subcortical projections to the dorsal cortical pathway (Fang and He, 2005). Arcaro et al. (2018) corroborated this speculation by showing that cortical tool regions were intrinsically functionally connected with the dorsal pulvinar. However, systematic investigations of whether and how the pulvinar processes visual stimuli with a domain pattern, and its relationship with the cortical domain distribution, are lacking.

To examine whether object domain organization is also present in the pulvinar, forming a cortical-subcortical domain network, we tested the pulvinar response patterns and cortical connectivity patterns associated with different domains of objects, focusing on animals and tools given the previous empirical observations about their potential sensitivity in the pulvinar. Conspecific neutral faces and large nonmanipulable manmade objects were included as reference conditions to depict the relative domain specificity. We focused on the pulvinar because of the previous clues of its sensitivity to various specific animate items, and because its size allows investigation using the current 3T fMRI resolution without compromising the whole-brain scan to understand the cortical-subcortical connectivity pattern. We combined fMRI activation experiments, resting-state connectivity analyses, and task-based dynamic causal modeling (DCM) to address the following questions: (1) whether the pulvinar shows significant, consistent activity patterns specifically associated with animals or tools relative to other objects; (2) if any potential animal and/or tool domain preferring activity patterns are discovered within the pulvinar, whether it is functionally connected with corresponding domain-preferring cortical regions, forming a domain-specific functional network; and (3) what the direction of information flow is within the pulvinar-cortical domain-preferring systems during visual processing.

Materials and Methods

Combining fMRI activation experiments, resting-state functional connectivity (RSFC) analysis and task-based DCM analysis, we investigated the object domain patterns in the pulvinar and its relation to the object domain distribution in the cerebral cortex. We first established the object domain selectivity profile in the pulvinar using a classical object domain localizer in Experiments 1 and 2, and then validated that profile through a series of other object domain experiments that covered similar object domains. These experiments included animal or tool object domain we collected previously (validation dataset 1–5, VD1-VD5) and the working memory experiment from Human Connectome Project (HCP). RSFC analysis was conducted to examine whether the pulvinar object domain preference topography corresponded to its functional connectivity pattern with the cortical object domain networks. DCM analysis was then conducted to examine the direction of the information flow within the pulvinar-cortical network of each domain.
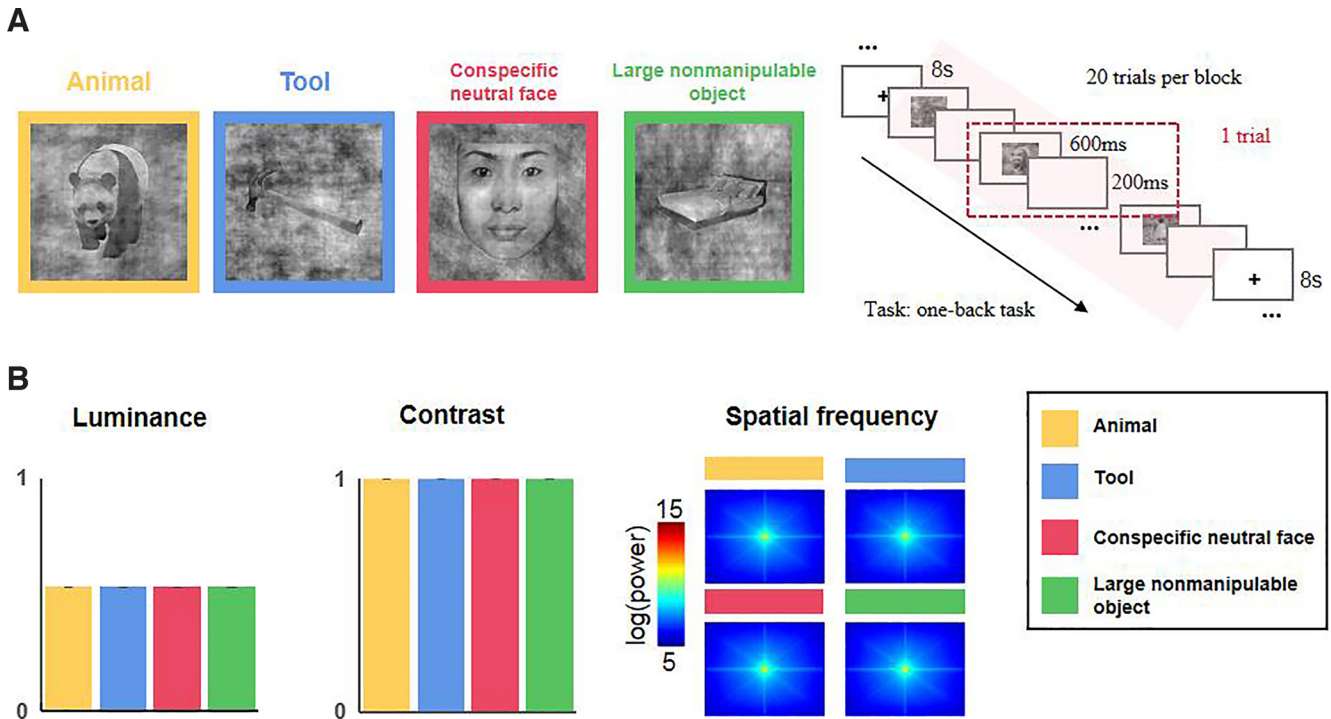
Experiments 1 and 2

Subjects. Twenty-one healthy college students (12 females; aged 19–35, mean age 23, SD 4) participated in Experiment 1, and 20 healthy college students (10 females; aged 18–27, mean age 22, SD 2) participated in Experiment 2. All subjects were right-handed, had normal or corrected-to-normal vision, and had no history of neurologic or psychiatric disorders. All subjects received monetary compensation for their participation. All subjects gave written informed consent to the experimental protocols, which were approved, respectively, by the Institutional Review Board of the National Key Laboratory of Cognitive Neuroscience and Learning, Beijing Normal University (Experiment 1) and by the Human Subject Review Committee at Peking University (Experiment 2).

Stimuli. In both Experiments 1 and 2, subjects viewed pictures from four object domains (20 items each): animals (mammals, insects, birds, reptiles), tools (everyday manipulable tools), large nonmanipulable manmade objects (furniture and other large fixed items), and conspecific neutral faces (for example stimuli, see Fig. 1A; for all stimuli pictures, see https://osf.io/6cgex/?view_only=7788e2dd7ee6442599461113af5f486b). Pictures for animals, tools, and large nonmanipulable objects were first selected from miscellaneous sources including the web and in house collections, and for faces from the "Chinese affective picture system" (Bai et al., 2005). Pulvinar has been shown to be sensitive to low-level image properties, such as color, luminance/contrast, spatial frequencies (Benevento and Miller, 1981; Öhman, 2005; Saalmann and Kastner, 2011). We thus further processed the images to match on these potential confounding variables across domains. Each item (grayscale, 400×400 pixels, visual angle: $10.55° \times 10.55°$ in Experiment 1; $7.6° \times 7.2°$ in Experiment 2) was placed on a phase-scrambled background generated from a selected picture from the other three object domains to minimize low-level image differences across object domains. The mean luminance, Michelson contrast, and spatial frequency of the pictures (Fig. 1B) were matched across domains using the SHINE toolbox (Willenbockel et al., 2010).

We further considered three lines of properties in which items of different domains may differ by collecting ratings in an independent subject group ($N = 26$) and computing mid/high-level image statistics. First, given that pulvinar has been suggested to be sensitive to stimuli of threat (Ward et al., 2007; Koizumi et al., 2019), we collected ratings on levels of threats, emotional valence, and arousal (7 point scale). The ratings of each item were averaged across subjects, and compared among object domains. Animals were higher on threatening and arousal ratings than other categories (p values < 0.05, except for threatening, animal vs tool, $p = 0.34$; Table 1) and largely comparable on the valence rating (animal vs face/tool, p values > 0.3; animal vs large nonmanipulable object, $p = 0.001$). Second, beyond the low-level image properties, objects of different domains tend to associate with certain mid-/high-level visual properties (e.g., Zachariou et al., 2018; Fan et al., 2021). For our stimuli pictures, we computed: mid-level shape properties (i.e., curvature, right angle, elongation), retinal size (following procedures described in Fan et al., 2021), and collected ratings on texture (i.e., smoothness, texturedness; following procedures in Baumgartner and Gegenfurtner, 2016). Third, we considered emergent (knowledge) properties by collecting ratings on real-world object size and familiarity (how familiar subjects were with the objects). Indeed, items of different domains showed differences across these higher-level properties (Table 1) in line with the literature (Konkle and Caramazza, 2013; Chen et al., 2018; Fan et al., 2021), with

Figure 1. Stimuli and experimental design in object domain experiments. **A**, Sample stimuli and experimental design in Experiment 1 (20 subjects) and Experiment 2 (21 subjects). In both experiments, images of 80 objects (20 animals, 20 tools, 20 conspecific neutral faces, and 20 large nonmanipulable objects) were used. In Experiment 1, each run consisted of 12 task blocks (3 for each domain), separated by 8 s intervals of a blank screen. Each block presented 20 pictures from a single domain, and each picture was presented for 600 ms, with an interstimulus interval of 200 ms. Experiment 2 had a highly similar design to that of the Experiment 1, except that each picture was presented for 300 ms with an interstimulus interval of 500 ms. **B**, Low-level visual feature computation of stimuli in Experiments 1 and 2. The luminance, contrast (Michelson contrast, calculated as the difference and sum of the maximum and minimum pixel intensities), and frequency of the images were well matched.

Table 1. Property results for the four object domains[a]

Properties	Animal	Tool	Conspecific neutral face	Large nonmanipulable object
Threatening	3.99 ± 1.48	3.52 ± 1.54	3.19 ± 0.48	2.07 ± 0.18
Emotional valence	3.53 ± 1.22	3.55 ± 0.81	3.82 ± 0.48	4.53 ± 0.45
Emotional arousal	4.78 ± 1.03	3.26 ± 1.24	3.62 ± 0.31	2.48 ± 0.31
Curvature	-0.40 ± 0.52	-0.26 ± 0.79	0.87 ± 0.47	-0.21 ± 0.65
Right angles	-0.49 ± 0.28	-0.05 ± 0.52	0.11 ± 0.35	0.42 ± 0.95
Elongation	1.47 ± 0.40	3.22 ± 1.15	1.15 ± 0.02	1.46 ± 0.41
Retina size	0.20 ± 0.06	0.09 ± 0.04	0.39 ± 0.03	0.25 ± 0.11
Smoothness	4.29 ± 0.90	3.14 ± 0.91	3.95 ± 0.55	3.06 ± 0.54
Texturedness	4.70 ± 0.76	2.56 ± 0.57	3.31 ± 0.23	2.82 ± 0.50
Real-word size	3.65 ± 1.74	1.81 ± 0.51	2.82 ± 0.18	4.82 ± 0.73
Familiarity	4.10 ± 0.87	6.01 ± 0.53	—	6.04 ± 0.48

[a]Threatening, emotional valence, arousal, smoothness, texturedness, real-world size, and familiarity were rated on 7 point scale, with 7 being more threatening, more positive, higher arousal, less smooth, more texturedness, larger, and more familiar, respectively; curvature and right-angle information was Z-scored across pictures during computation (for details, see Fan et al., 2021); retina size (pixel number ratio) was defined as the proportion of object pixels in all pixels; elongation was measured as the aspect ratio of the rectangle that covering the object along the longest axis.

animals being less smooth and more textured (smoothness, animal vs large nonmanipulable object/tool, p values < 0.001, animal vs face, $p = 0.16$; texturedness, all p values < 0.001) and tools being more elongated and having smaller pixel number ratio (elongation, pixel number ratio, all p values < 0.001). Results will be considered in light of such property differences.

Experimental design. In Experiment 1, fMRI data were acquired when subjects viewed pictures from the four object domains over four block-design runs (Fig. 1A). Each run lasted for 300 s, began and ended with a 10 s fixation period, during which a fixation was presented at the center of the screen. Each run consisted of 12 task blocks (three for each

object domain), separated by 8 s intervals of a blank screen. Each block presented 20 pictures from a single object domain, and each picture was presented for 600 ms, with an interstimulus interval of 200 ms. The subjects were instructed to look at the pictures carefully and to press a button with their right index finger as soon as they detected a picture that appeared twice in a row (one-back task). Within each block, the planned number of button presses was 0, 1, or 2. The total number of planned button presses was matched across object domains and runs. The presentation order of pictures within each block was randomized, and the order of runs was counterbalanced across subjects.

Experiment 2 had a highly similar design to Experiment 1. The only difference was the trial structure: in Experiment 2, each picture was presented for 300 ms, with an interstimulus interval of 500 ms. In Experiment 2, subjects took an 8-min-long (240 volumes) resting-state fMRI scan before task-fMRI scanning, during which the subjects were asked to close their eyes and to not fall asleep.

Image acquisition. Data of Experiment 1 were collected on a 3T Siemens Trio Tim scanner with a 64-channel head-neck coil at the Imaging Center for Brain Research, Beijing Normal University. Functional images were acquired using an EPI sequence (33 axial slices, TR = 2000 ms, TE = 30 ms, flip angle (FA) = 90°, matrix size = 64 × 64, voxel size = 3 × 3 × 3.5 mm³ with gap of 0.7 mm). High-resolution 3D T1-weighted images were acquired using the 3D-MPRAGE sequence (144 sagittal slices, TR = 2530 ms, TE = 3.39 ms, FA = 7°, matrix size = 256 × 256, voxel size = 1.33 × 1.0 × 1.33 mm³).

Data of Experiment 2 were collected on a 3T Siemens Prisma scanner with a 64-channel head-neck coil at the Center for MRI Research, Peking University. The functional images were acquired using a multiband EPI sequence (62 axial slices, TR = 2000 ms, TE = 30 ms, FA = 90°, FOV = 224 mm × 224 mm, matrix size = 112 × 112, slice thickness = 2.0 mm, voxel size = 2 × 2 × 2 mm³ with gap of 0.3 mm, multiband factor = 2). High-resolution 3D T1-weighted images were acquired using the 3D-MPRAGE sequence (192 sagittal slices, TR = 2530 ms, TE = 2.98 ms, TI = 1100 ms, FA = 7°, FOV = 256 mm × 224 mm, matrix

size = 224 × 256, interpolated to 448 × 512, slice thickness = 1.0 mm, voxel size = 0.5 × 0.5 × 1 mm³).

Data preprocessing. Task fMRI data were preprocessed using Statistical Parametric Mapping software (SPM12; http://www.fil.ion.ucl. ac.uk/spm/software/spm12/). No subject exhibited excessive head motion in either experiment (>3 mm maximum translation or 3° rotation in Experiment 1 and >2 mm/2° in Experiment 2). After the first five volumes of each functional run were discarded for signal equilibrium, the functional data underwent slice timing, head motion correction, and normalization into the MNI space using unified segmentation. The resulting functional images with isotropic voxels (3 mm for Experiment 1; 2 mm for Experiment 2) were further spatially smoothed with a 4 mm FWHM Gaussian kernel.

Resting-state fMRI data were preprocessed using SPM12, the toolbox for Data Processing & Analysis for Brain Imaging (version 5.1) (Yan et al., 2016) and analyzed using the resting-state fMRI Data Analysis Toolkit version 1.8 (Song et al., 2011). No subject exhibited excessive head motion (>2 mm maximum translation or 2° rotation). For each subject, preprocessing follows conventional procedures, which include the following: (1) discarding the first 5 volumes for signal equilibrium; (2) slice timing; (3) correcting for head movement; (4) regressing out nuisance variables, including the global signal averaged across the whole brain, mean white matter (WM), the CSF signals, and continuous head movement (Friston-24 parameters) (Friston et al., 1996) to further reduce non-neuronal signal confounds; (5) removing the signal trend with time linearly; (6) bandpass (0.01-0.1 Hz) filtering; (7) normalization into MNI space by DARTEL (Ashburner, 2007); and (8) spatial smoothing with a 4 mm FWHM Gaussian kernel.

Data analysis

For each individual subject, the preprocessed task-functional images were entered into a GLM. For each run, the GLM included four regressors of interest corresponding to the four object domains, each convolved with the canonical HRF. The GLM also included six head motion parameters as regressors of no interest. The high-pass filter was set at 128 s. After model estimation, whole-brain contrast images of each object domain versus baseline were calculated for each subject. The contrast images of each object domain versus the average of other object domains were also calculated to measure the object domain effect at the individual level.

Definition of the pulvinar mask. The pulvinar mask was defined anatomically as the combination of the bilateral medial pulvinar (PuM), inferior pulvinar (PuI), lateral pulvinar (PuL), and anterior pulvinar (PuA) regions from the 3D atlas of the human thalamus (Krauth et al., 2010). The pulvinar mask was resliced to match the corresponding spatial resolution of each experiment, resulting in 170 pulvinar voxels (left: 83, right: 87; voxel size = 3 mm³) for Experiment 1and 595 pulvinar voxels (L: 297, R: 298; voxel size = 2 mm³) for Experiment 2.

Univariate analyses. We first performed a univariate group analysis (van den Hurk et al., 2017; Striem-Amit et al., 2018; Mattioni et al., 2020) in the predefined pulvinar mask. Specifically, we averaged the responses (β values) for each condition across sessions and subjects on each voxel and determined which condition generated the strongest mean response. A paired t test was then conducted across subjects on each voxel to compare the object domain with the strongest mean response with the mean responses of the other three domains, and the t statistic was assigned to the voxel. False discovery rate (FDR) multiple comparison corrections were then undergone for the resulting t-statistic maps ($q = 0.05$) in the pulvinar. For Experiment 2, in addition to the stringent threshold, a more lenient threshold was set (voxel $p = 0.01$, $k = 10$) for visualization.

We also depicted the winner-take-all maps within the pulvinar. For each domain, the mean response (β values across all voxels in pulvinar) was subtracted from each voxel's β. The domain with the strongest (mean-centering) normalized β value was assigned to each voxel. This normalizing method highlighted the clusters of voxels whose selectivity for a particular condition was distinguished from the surrounding others (following van den Hurk et al., 2017). For each domain, voxels in each hemisphere were counted, and χ^2 tests were conducted to test the potential difference.

We tested the consistency of the domain distributions across the two experiments using multiple approaches. Additionally, we computed the agreement between the winner-take-all maps of the two experiments using Cohen's κ coefficient (Cohen, 1960) to check whether the domain distributions were consistent across experiments. The winner-take-all map of Experiment 2 was resliced to the spatial resolution of Experiment 1 to perform correlation analysis. The consistency between the winner-take-all maps without normalization was also computed in a similar manner.

We also computed the consistency between the two experiments directly for animals and tools (t map, each domain vs the average of the other three object domains). Taking animal, for example, we compared the correlation between the animal t maps across two experiments (within-domain, between experiments) to the correlations between the animal t map from one experiment and the t maps of other object domains from the other experiment (between domains and experiments). Permutation tests were used for statistical testing. For each object domain and for the two experiments, the t values within the pulvinar were scrambled randomly, and the difference between the within-domain, between-experiment correlation and the between-domain, between-experiment correlations was computed. This process was repeated 10,000 times, producing distributions for each comparison. The differences computed based on the actual data were then compared against these distributions. Comparisons for the tool condition were computed in a similar manner.

Laterality computation. To measure the lateralization of object domain-related responses, we computed the laterality index (LI) using the LI toolbox (Wilke and Lidzba, 2007). The t maps of each object domain versus the average of the other object domains were entered as inputs to compute LI curves using a bootstrapping method ($n = 10,000$) with the following options: a bilateral pulvinar inclusive mask, no exclusive masking, and the default bootstrapping parameters. This method involved the calculation of 20 equally sized thresholds from 0 to the maximum t value. At each threshold, 100 bootstrapped samples were taken in the left and the right ROIs, respectively (200 in total). All 10,000 possible LI combinations (100 samples in the left ROIs × 100 samples in the right ROIs) were then calculated from these samples in surviving voxels using the formula $[(L - R)/(L + R)]$. Only the central 50% of the data were kept to exclude statistical outliers. A weighted mean LI was then calculated for each image for all LIs weighted with their corresponding thresholds. The mean weighted LI index varied from -1 to 1, with -1 being completely right-lateralized and 1 being completely left-lateralized, and values between -0.2 and 0.2 being considered to be bilateral (Seghier, 2008; for a more lenient cutoff of laterality $[|LI| > 0.1]$, see Szaflarski et al., 2006).

Group LIs were calculated for the pulvinar separately for each domain. We also computed the LIs for each domain in each subject. One-sample t test analyses (against zero) were conducted to test whether the lateralization was reliable at the individual level. The Cohen's d effect sizes were additionally computed for the significant t test results.

Validation datasets. To validate the lateralization effects in the pulvinar observed in Experiments 1 and 2, we reanalyzed the data of five object domain experiments from our previous studies (summarized in Fig. 3A). Only VD2 was not published previously, and the information is as follows: VD2 consisted of data from a single run localizer when 25 subjects viewed blocks of tools and animals (unpublished data). The run lasted for 7 min and 32 s, beginning with a 10 s fixation and ending with a 12 s fixation, during which a fixation was presented at the center of the screen. There were 20 task blocks (10 for each object domain), separated by 10 s intervals of a blank screen. Each block presented 12 pictures from a single object domain, and each picture was presented for 500 ms, with an interstimulus interval of 500 ms. The subjects were instructed to look carefully and to press a button with their right index finger as soon as they detected a picture that appeared twice in a row. The presentation order of pictures within each block was randomized. We performed the same preprocessing reported in previous studies, except that spatial smoothing was conducted with a 4 mm FWHM Gaussian kernel (for more detailed experimental descriptions, see our previous publications).

We also analyzed data from the WU-Minn HCP (https://www.humanconnectome.org/study/hcp-young-adult; approved by the Institutional Ethics Committee of Washington University, St. Louis, Missouri) (Van Essen et al., 2013). For the current analyses, we used the fMRI data of the working memory task, which included stimuli from four object domains (i.e., faces, places, tools, and body parts) (Barch et al., 2013). We used the minimally preprocessed images (for detailed preprocessing procedure, see Glasser et al., 2013), which were further spatially smoothed with a 4 mm FWHM Gaussian kernel. Other data processing (i.e., constructing a GLM, contrasting object domains, and conducting the group analyses) was the same as that of Experiments 1 and 2. We did not differentiate between the task conditions (i.e., 0-back, 2-back) that the working memory experiment included. A total of 910 subjects were identified, as they did not exhibit excessive head motion (>2 mm maximum translation or 2° rotation) or any data quality issues, as reported in the HCP project manual (https://www.humanconnectome.org/storage/app/media/documentation/s1200/HCP_S1200_Release_Reference_Manual.pdf). The analysis was confined to the individuals who were right-handed (handedness index > 40, $N = 786$) (Arshad et al., 2013). Tool activation was not localized in four individuals, and the remaining 782 subjects entered the individual analysis. We also validated our results on 392 individuals (discarding those that were in the sibling cohorts) to further rule out the intersubject dependence caused by genetic similarity.

Resting fMRI connection analysis. We tested the communication between the pulvinar and cortical object domain regions using the object picture viewing fMRI data from Experiment 1, and the resting-state fMRI data collected from an independent group of 144 right-handed healthy young subjects (described by H. Yang et al., 2017). All subjects gave written informed consent to the experimental protocols, which were approved by the Institutional Review Board of the National Key Laboratory of Cognitive Neuroscience and Learning, Beijing Normal University. The scan lasted for 6 min and 40 s, during which the subjects were asked to close their eyes and to not fall asleep. The preprocessing steps included the removal of the first 10 volumes, slice timing, motion correction, spatial normalization into MNI space using unified segmentation (resampling voxel size was $3 \times 3 \times 3$ mm^3), linear trend removal, bandpass filtering (0.01-0.1 Hz), spatial smoothing (6 mm FWHM Gaussian kernel), and regression of nuisance variables (including six rigid head motion parameters, the global signal, the white matter signal, and the CSF signal). Given the controversy regarding the global signal regression (Liu et al., 2017; Murphy and Fox, 2017), we also performed the analysis without regressing out global signal.

We first identified cortical regions showing significant domain selectivity by contrasting each object domain with the average of the other three domains in the whole brain in Experiment 1. For each object domain, all cortical regions that survived the threshold of voxel-level $p < 0.001$, one-tailed, cluster-level family-wise error (FWE)-corrected $p < 0.05$ were collectively defined as the corresponding domain-selective "cortical seed ROI" (Fig. 4A). The overlapping voxels between cortical regions from different domains and the overlapping clusters between cortical regions and pulvinar were excluded from the subsequent analysis. As Figure 4A shows, mean time series were calculated by averaging the time series extracted from all voxels in each corresponding domain-selective "cortical seed ROI" for each subject in the independent resting fMRI data ($N = 144$). For each object domain, a cortico-pulvinar connectivity map was generated by correlating the time series of the corresponding domain cortical seed and the time series of each pulvinar voxel, while regressing out the time series from the other three object domain cortical seeds. The resulting r maps were further Fisher-transformed and tested against zero across subjects. The resulting t maps were defined as domain-specific cortico-pulvinar RSFC maps and were further correlated with the object domain activation maps in Experiment 1 (t map, each specific object domain vs the average of the other three object domains) to examine whether the cortico-pulvinar RSFC pattern corresponded to the object domain activation pattern. To statistically test the domain specificity of the RSFC-activation correspondence, we compare the within versus between domain correlations: correlations between the animal cortico-pulvinar RSFC map and the animal domain activation map versus

correlations between the animal cortico-pulvinar RSFC map and the other three object domain activation maps and correlations between the animal object domain activation map and the other three object domain-specific cortico-pulvinar RSFC maps, using the Hotelling's t test (the FZT computator, http://psych.unl.edu/psycrs/statpage/regression.html). Comparisons for tools were computed in the same manner.

We also collected the RSFC data of subjects in Experiment 2, and thus performed this analysis (task fMRI and RSFC relationship) using RSFC and fMRI activation data from the same group of subjects. The procedure was the same except that to include the frequently reported fusiform face area when viewing neutral face images, we defined the face-selective cortical seed under a more lenient threshold (voxel-level $p < 0.01$, one-tailed, cluster-level FWE-corrected $p < 0.05$).

DCM analysis
To determine the direction of information flow across the pulvinar-cortical domain-preferring systems, we performed DCM analysis using DCM12 (Friston et al., 2003) in the SPM12 software. DCM analysis allows us to investigate the direction of information flow between the pulvinar and cortical domain regions, and most importantly explore whether and how certain object domain modulates the directional connection (Penny et al., 2010; Stephan et al., 2010; Zeidman et al., 2019a, b). DCM is a hypothesis-driven technique. Models with different hypotheses of neural connectivity are constructed at the beginning, and then tested using Bayesian Model Selection (BMS) to decide which model or which family of models provides the most likely explanation of the observed data.

In the present study, we focused on how processing animals and tools stimuli modulated the intrinsic connectivity between the pulvinar and the corresponding cortical domain clusters. We were especially interested in whether the directional connections between pulvinar and cortical domain clusters were modulated by corresponding object domain. Based on our interest and for the sake of simplicity, we constructed models with only three ROIs: the pulvinar, primary visual cortex (V1), and object domain cortical ROIs. Different object domain cortical ROIs were tested separately, with only one ROI tested at a time. The external perturbation (all the four object domains) entered our model through both the pulvinar and V1. We considered all possible combinations of connections between the object domain cortical ROI and the pulvinar, and between the object domain cortical ROI and the visual primary cortex (Fig. 5A, no connection, only forward connection, only backward connection, or both forward and backward connections, combined with only intrinsic connection or object domain modulation connection), giving us a comprehensive model space of 80 models (models having no connection between either two regions were deleted). No intrinsic connection was defined between the pulvinar and V1 (McFadyen et al., 2019, 2020). The experiment input was mean-centered, which means that the intrinsic connection represented the average effective connectivity across object domain conditions and modulation connection was added to or subtracted from this average (Zeidman et al., 2019a). The model was estimated for each run for each subject. As we focused on the pulvinar-cortical communication, we further grouped our models into 9 families (Fig. 5A, Family A to Family I) according to the presence of intrinsic connections and modulation between the pulvinar and cortical clusters. The DCM analyses were conducted on Experiment 2 data with higher spatial resolution to ensure the inclusion of an adequate number of voxels.

For the tool domain, a left-lateralized cortical tool network was defined by contrasting tools with the average of the other three object domains (voxel-level $p < 0.001$, cluster-level $p < 0.05$, FWE-corrected), including ROIs in the lateral occipitotemporal cortex (LOTC, peak MNI coordinates: −46, −66, −4), the medial fusiform gyrus (FG, peak MNI coordinates: −26, −64, −16), and the superior parietal lobe (SPL, peak MNI coordinates: −38, −46, 60). Left V1 (peak MNI coordinates: −14, −100, 0) was defined by contrasting all object domain conditions versus resting baseline within the Brodmann mask (area 17) (Maldjian et al., 2003) restricted to the left hemisphere. For these areas, we defined the group ROI by placing spheres with a radius of 8 mm around corresponding peak coordinates. For the pulvinar, we used the predefined left

pulvinar mask as the group ROI. We then searched for the peak tool-selective activations (i.e., tool vs the average of other three domains) within the group ROIs in each individual subject. One subject was excluded because no voxel survived the height threshold of uncorrected $p < 0.05$. Single-subject ROIs were then constructed as spheres (radius = 3 mm, 19 voxels) centered on each subject's peak coordinates. A BOLD time series was obtained for each subject, and each ROI using the voxels that survived the uncorrected $p < 0.05$ in single-subject ROIs.

For the animal network, to include more animal-related areas (e.g., left FG), we defined animal ROIs using the contrast between animals versus large nonmanipulable object and tool conditions (voxel $p < 0.001$, FWE-corrected $p < 0.05$). We found selective activation to animals outside the bilateral pulvinar in the bilateral lateral occipital cortex (LO, MNI coordinates: left LO, −48, −80, 6; right LO, 50, −74, 0) and the bilateral FG (MNI coordinates: left FG, −42, −50, −24; right FG, 40, −48, −20). Using the all-object domain conditions versus resting baseline contrast combined with the Brodmann mask (area 17), we defined the left V1 and right V1 (MNI coordinates: left V1, −14, −100, 0; right V1, 26, −96, 10). For these areas, we defined the group ROI by placing spheres with a radius of 8 mm around these coordinates. As previous studies found that both the left and right amygdala responded to animals (both threatening and neutral animals) (Mormann et al., 2011; J. Yang et al., 2012), together with the evidence that the amygdala interacted with the pulvinar (Pessoa and Adolphs, 2010), we also included the amygdala as ROIs using the anatomic AAL mask (Amygdala_L, AAL 41; Amygdala_R, AAL 42) (Tzourio-Mazoyer et al., 2002). For the pulvinar, we used the pulvinar mask we described previously. We then searched for the individual peak coordinates within the group ROIs using the animal versus large nonmanipulable manmade objects and tool contrast. The procedures of discarding subjects and extracting time series were the same as those of the tool network analyses. For analyses of left OC and left FG, 3 subjects were discarded because no voxel survived the threshold of voxel $p < 0.05$, uncorrected in the left pulvinar, while for analyses of the right OC and right FG, 1 subject was discarded because no voxel survived the threshold of voxel $p < 0.05$ of the right pulvinar. For analyses of the left amygdala and right amygdala, 1 subject was discarded from each, as no voxel survived the extent threshold of voxel $p < 0.05$ of itself.

The previously described nine model families, representing nine competing hypotheses, were compared using random effect BMS. When comparing model families, all models within a family were averaged using Bayesian Model Averaging, and an exceedance probability was calculated for each family. The winning family was defined as the one with the highest exceedance probability. In the present study, as our interest was the relationship between the pulvinar and the cortex (or the amygdala), BMS was first performed on the nine model families with different pulvinar-cortical communication types (Fig. 5). BMS performed on 80 models, choosing the best model, were also conducted for validation.

Data and materials availability
The data that support the findings of this study are available at https://osf.io/6cgex/?view_only=7788e2dd7ee6442599461113af5f486b.

Results
The following three lines of results were reported: (1) To test whether the pulvinar showed significant, consistent sensitivity pattern associated with animals and/or tools, two fMRI picture viewing experiments were performed. The observed domain sensitivity pattern was validated using five in-house, previously collected datasets, and using the HCP dataset. (2) To test the relationship between cortical and pulvinar animal/tool preference distributions, the cortico-pulvinar RSFC map was computed, and its relationship with pulvinar domain activation pattern was examined. (3) To test the direction of information flow within the pulvinar-cortical network for each domain (i.e., among the pulvinar and cortical domain-preferring clusters), the DCM analysis was conducted on the task-state fMRI data.
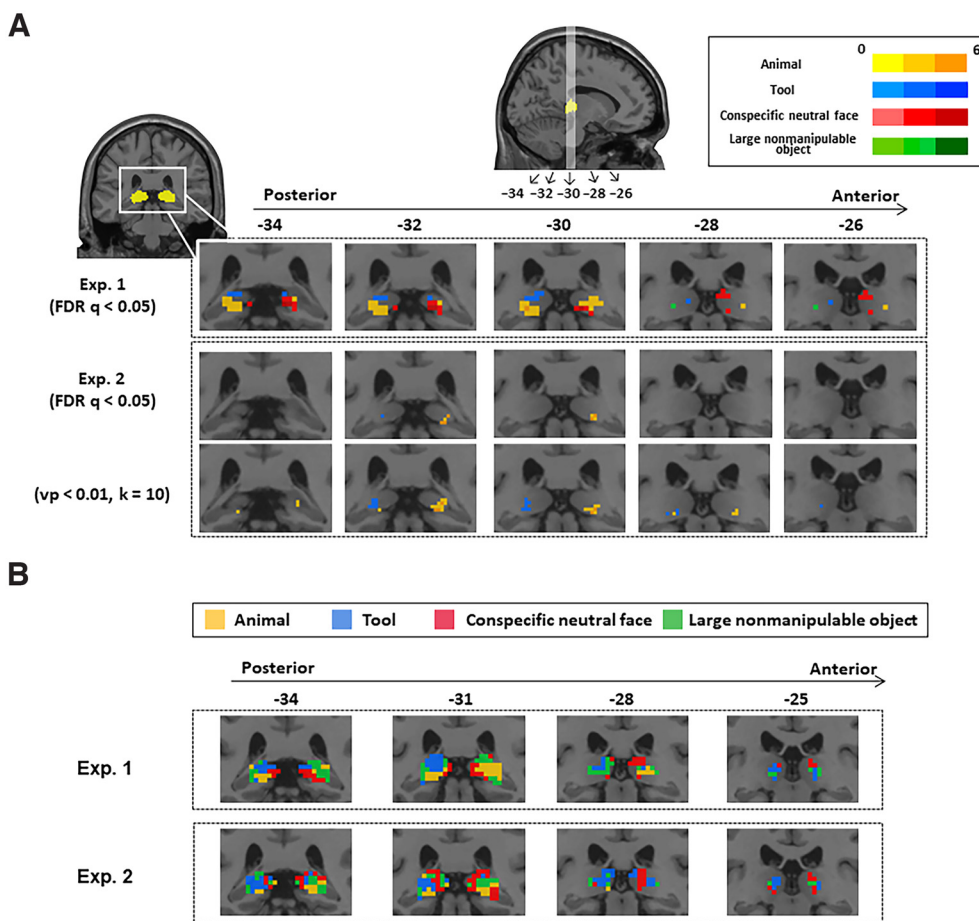
Object domain-preferring activity topography in the pulvinar
Two object domain experiments with identical stimuli, with varying design and scanning parameters, were conducted for replication. In both experiments, subjects viewed pictures belonging to four commonly studied object domains (animals and tools, along with conspecific neutral faces and large nonmanipulable objects as references, Fig. 1A) and detected whether a picture appeared twice in a row (i.e., the one-back task; Fig. 1A). Experiment 2 had a higher spatial resolution ($2 \times 2 \times 2$ mm^3) than Experiment 1 ($3 \times 3 \times 3$ mm^3), which allowed finer spatial scale examination of object domain effects in the pulvinar. All pictures were matched for low-level visual features, including mean luminance, contrast, and spatial frequency (Fig. 1B).

Experiment 1 results
We performed a univariate group analysis on the picture viewing responses in the pulvinar (see Materials and Methods). Paired t tests contrasting each object domain against the average of the other three object domains across subjects revealed voxels showing significant preferences for animals and tools (Fig. 2A, FDR $q < 0.05$ confined to the pulvinar). The animal-preferring voxels showed up in both hemispheres, distributed ventral to the tool-preferring voxels and lateral to the face-preferring voxels, and the tool-preferring voxels were predominantly located in the dorsal part of the left pulvinar (Fig. 2A; Table 2; animal voxels in the two hemispheres were not statistically different in quantity: right pulvinar, $n = 10$, left pulvinar, $n = 18$, $\chi^2 = 2.29$, $p = 0.13$, df = 1). More tool voxels were found in the left hemisphere than in the right hemisphere (right pulvinar, $n = 1$, left pulvinar, $n = 9$, $\chi^2 = 6.40$, $p = 0.01$, df = 1). To further visualize the relative domain preferences across the four object domains on the same map, we additionally created a winner-take-all map, where for each voxel the object domain with the strongest response (group-mean normalized) for each voxel was assigned to it (Fig. 2B; see Materials and Methods). The tool-highest voxels again showed a strong left laterality (right pulvinar, $n = 7$, left pulvinar, $n = 34$, $\chi^2 = 17.78$, $p < 0.001$, df = 1), and the animal-highest voxels were confined to the ventral part of the pulvinar and bilaterally distributed (right pulvinar, $n = 24$, left pulvinar, $n = 15$, $\chi^2 = 2.08$, $p = 0.15$, df = 1).

Experiment 2 results
We then tested the object domain preference in Experiment 2 with a higher spatial resolution. Paired t test again found animal-preferring voxels and tool-preferring voxels (Fig. 2A; Table 2, FDR $q < 0.05$ confined to the pulvinar; results were also shown at a lower threshold, $p < 0.01$, $k = 10$, for voxel pattern illustration). The animal-preferring voxels appeared in both hemispheres again and were distributed mainly in the ventral part of the right pulvinar (voxel $p < 0.01$, $k = 10$, with significantly more animal voxels found in the right hemisphere than in the left hemisphere: right pulvinar, $n = 25$, left pulvinar, $n = 3$, $\chi^2 = 17.29$, $p < 0.001$, df = 1), and the tool-preferring voxels were confined to the left pulvinar (right pulvinar, $n = 0$, left pulvinar, $n = 18$). In the winner-take-all map (Fig. 2B), the tool-highest voxels again showed a strong left laterality (right pulvinar, $n = 40$, left pulvinar, $n = 123$, $\chi^2 = 42.26$, $p < 0.001$, df = 1), and the animal-highest voxels were relatively right-lateralized (right pulvinar, $n = 71$, left pulvinar, $n = 47$, $\chi^2 = 4.88$, $p = 0.027$, df = 1). The results of the two experiments were significantly consistent: The winner-take-all maps were significantly correlated (Cohen's $\kappa = 0.19$, $p < 0.001$; without normalization as in Fig. 2A: Cohen's $\kappa = 0.13$, $p = 0.023$). The within-domain correlations for the

Figure 2. Object domain-preferring activity topography in the pulvinar. ***A***, Object domain-preferring activity topography in the pulvinar. The pulvinar mask (yellow) was presented in coronal (top left) and sagittal (top middle) slice views. The thresholded activation pattern of the pulvinar is shown in coronal views from posterior to anterior with MNI *y* coordinates denoted. Color bars in the top right inbox represent the *t* values of the domain preference contrast (each domain vs the average of the other three). Experiment 1 (3 mm³ resolution) and Experiment 2 (2 mm³ resolution) are shown in the top and bottom panels, respectively. ***B***, Winner-take-all maps in the pulvinar in Experiments 1 and 2. Color of each voxel represents the domain that induces the highest activation across all domains in the corresponding voxel. The maps are presented in the same resolution (3 mm³) for visual comparison.

Table 2. Object domain preference results for the pulvinar in Experiments 1 and 2

	Object domains	Peak voxel (T value)	Cluster size (voxels)	MNI coordinates		
				x	*y*	*z*
Experiment 1 (FDR voxel *p* < 0.05, confined to the pulvinar)	Animal vs others	4.38	18	−21	−30	0
		3.49	10	18	−30	3
	Face vs others	5.48	11	12	−33	0
		3.25	1	−9	−33	0
		3.21	6	6	−27	9
	Large nonmanipulable object vs others	2.34	1	−21	−27	3
	Tool vs others	3.87	9	−18	−33	6
		2.47	1	12	−33	6
Experiment 2 (FDR voxel *p* < 0.05, confined to the pulvinar)	Animal vs others	5.30	8	18	−30	−2
	Face vs others	—	—	—		
	Large nonmanipulable object vs others	—	—	—		
	Tool vs others	3.91	1	−20	−32	2
Experiment 2 (voxel *p* < 0.01, *k* > 10)	Animal vs others	5.30	25	18	−30	−2
		3.08	2	−16	−34	−2
		2.54	1	−18	−28	0
	Face vs others	—	—	—		
	Large nonmanipulable object vs others	—	—	—		
	Tool vs others	3.91	15	−20	−32	2
		3.32	3	−16	−26	2

domain preference statistical maps across two experiments (animal $r = 0.32$, $p < 0.001$; tool $r = 0.28$, $p < 0.001$) were significantly larger than between-domain correlations across experiments (for animals: p values < 0.01; for tools: p values < 0.001, except $p = 0.11$ for within tools vs between large objects-tools).

Reference object domain results

For the two reference object domains (conspecific neutral faces and large objects), the large objects induced negligible pulvinar responses compared with other object domains in both experiments (Fig. 2A). The neutral face preference was inconsistent between experiments. In Experiment 1, face-preferring voxels were observed predominantly in the medial part of the right pulvinar (Fig. 2A; Table 2, $\chi^2 = 14.22$, $p < 0.001$, df = 1). In Experiment 2, no voxel showed above-threshold preference for conspecific neutral faces even under the most lenient threshold of voxel $p < 0.01$, $k = 10$. Looking at the winner-take-all maps for the two experiments, there was a consistent right-hemisphere preference for neutral faces (Fig. 2B, Experiment 1: right pulvinar, $n = 28$, left pulvinar, $n = 10$, $\chi^2 = 8.53$, $p = 0.004$, df = 1; Experiment 2: right pulvinar, $n = 125$, left pulvinar, $n = 45$, $\chi^2 = 37.65$, $p < 0.001$, df = 1). In the analyses below, we focused on the animal and tool domains given their robust activation results and the theoretical interest explained in the Introduction.

LI results: robust laterality of object domain preference in the pulvinar

In the analyses above, we consistently observed that the tool-preferring voxels tended to be found in the left hemisphere, while the animal-preferring voxels tended to be more bilaterally distributed (Experiment 1) or right-lateralized (Experiment 2). Here, we quantify this observation by computing the LI for each domain using the LI toolbox (Wilke and Lidzba, 2007) implemented in SPM12 (for details, see Materials and Methods). The LIs were computed based on the t maps of each object domain versus the average of the other three object domains at both the group level and the individual level. The LI varies between the range from -1 to 1, with -1 being completely right-lateralized, 1 being completely left-lateralized, and values between -0.2 and 0.2 considered as bilateral (Seghier, 2008; for a more lenient cutoff of laterality [$|LI| > 0.1$], see Szaflarski et al., 2006).

Group lateralization results

Consistent with the object domain preference and winner-take-all maps, the pulvinar showed strong left laterality of tool-preferring voxels at the group level in both experiments (Experiment 1: 0.83; Experiment 2: 0.61). The animal-preferring voxels in the pulvinar were evenly distributed between the hemispheres in Experiment 1 and were right-lateralized in Experiment 2 (Experiment 1: 0.05; Experiment 2: -0.26).

Individual lateralization results

We further tested whether the object domain preference lateralization was reliable at the individual subject level. For each object domain, one-sample t tests were conducted against zero on the LIs computed from the t maps of individual subjects. As shown in Fig. 2, the results revealed significantly left-lateralized tool preference (Fig. 3B, Experiment 1: mean LI = 0.25, $t = 3.11$, $p = 0.005$, df = 20, Cohen's $d = 0.68$; Experiment 2: mean LI = 0.20, $t = 2.74$, $p = 0.013$, df = 19, Cohen's $d = 0.61$) across subjects in both experiments. There was no significantly lateralized animal preference in either Experiment 1 (Fig. 3B, Experiment 1: mean LI = -0.04, $t = -0.49$, $p = 0.63$, df = 20) or Experiment 2

(mean LI = -0.03, $t = -0.46$, $p = 0.65$, df = 19). Individual LIs are also presented in the bar plot in Figure 3B. Together, across the two experiments of differing spatial resolution, we observed relatively consistent left-lateralized tool preference in the pulvinar across individual subjects, while no clear, consistent laterality effects were observed for animals across subjects.

Validation of the lateralization effects in the pulvinar across multiple datasets

In both Experiments 1 and 2, lateralization was the most consistent and salient functional specialization pattern for different object domains in the pulvinar. To further validate this effect, we reanalyzed the data of five previously conducted experiments from our laboratory (of which four were published) that included picture viewing of animals and/or tools (He et al., 2013; Wang et al., 2016, 2017, 2018; Wu et al., 2020; Fan et al., 2021), yet did not scrutinize the pulvinar effects at the time. In four of the five experiments, tools showed left lateralization in pulvinar in the group analysis (Fig. 3C, LI: VD1, 0.91; VD2, 0.41; VD3, 0.66; VD4, 0.49). The VD5 (LI: 0.13) also showed a left lateralization trend in a more lenient cutoff of laterality ($|LI| > 0.1$, Szaflarski et al., 2006). The animals showed a right preference in three of the four validation datasets (VD3 did not contain animals; Fig. 3C, LI: VD1, 0.28; VD2, -0.42; VD4, -0.36; VD5, -0.59). The left lateralization of animals in VD1 was caused by the strong right lateralization of faces in this dataset. When excluding the face category, animals (vs the average of large objects and tools) still showed a right lateralization (LI = -0.2). Pooling all subjects together (115 individuals for tools and 96 for animals), one-sample t tests showed that the pulvinar showed left lateralization for tools (Fig. 3C, $t = 3.27$, two-tailed $p = 0.001$, df = 114, Cohen's $d = 0.30$) and a right preference for animals (Fig. 3C, $t = -2.31$, two-tailed $p = 0.02$, df = 95, Cohen's $d = -0.24$). We also analyzed data from the HCP dataset (subject $N = 782$) (Van Essen et al., 2013). This datatset included a picture viewing task with four object domains including a "tool" condition (although not all typical tools as investigated in our experiments), faces, scenes and body parts, but did not contain animals. A strong left lateralization for tools was again found in the group results (LI = 0.41). The effects were also highly robust in the individual analyses (Fig. 3C, $t = 3.79$, two-tailed $p < 0.001$, df = 781, Cohen's $d = 0.14$). These results held when we excluded genetically related individuals (who were twins or non-twin siblings) (remaining $N = 392$; $t = 2.76$, two-tailed $p = 0.006$, df = 391, Cohen's $d = 0.14$).
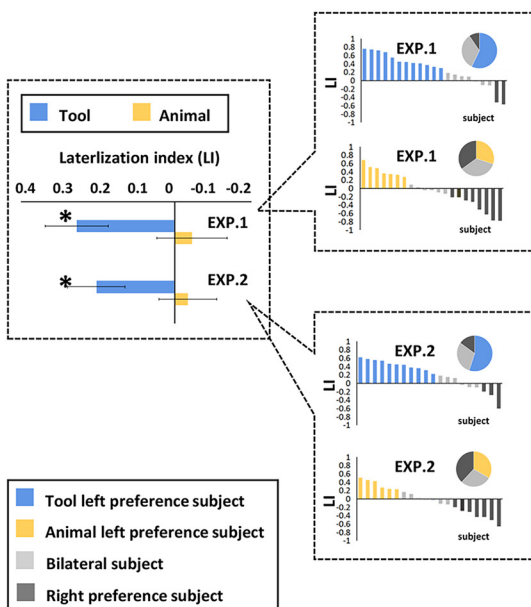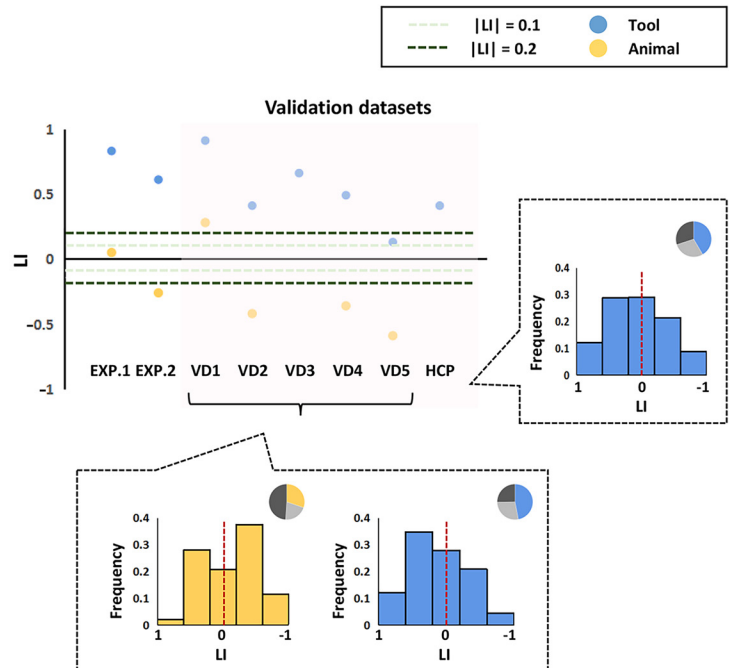
RSFC results: the cortico-pulvinar RSFC pattern aligns with the animal and tool domain pulvinar activation pattern

Now that we have observed domain-sensitive patterns in the pulvinar for tools and animals, do they associate with the corresponding domain preference clusters in the cortex? We used an independent resting-state fMRI dataset ($N = 144$) (H. Yang et al., 2017) to test the intrinsic functional connectivity pattern between the pulvinar and cortex.

We first defined cortical regions showing significant preference for the corresponding domain in Experiment 1 as the "cortical seed network" (Fig. 4A, vs the average of the other three object domains, voxel-level $p < 0.001$, one-tailed, cluster-level FWE-corrected $p < 0.05$). Animal cortical seed network included left and right lateral fusiform and occipital areas. Tool cortical seed network included LOTC, parietal, medial fusiform, and occipital areas. We then computed the Pearson correlation between the mean time series of each cortical seed network (i.e.,

Figure 3. Robust laterality of object domain preferences in the pulvinar. *A*, Summary of validation datasets. *B*, Lateralization in the pulvinar at the individual level. Bar plots represent the LI for animals and tools in the pulvinar. Asterisks were shown when the LIs of the animal or tool conditions across individuals are significantly higher than zero. Error bars indicate SEs. Individual LIs for animals and tools are further shown on the right side, with the pie chart showing the population proportion of lateralization preference (|LI| > 0.2). The subjects are sorted according to their LI index for each object domain condition in each experiment. *C*, Lateralization in the pulvinar at the group level. The animal and tool group LIs for Experiment 1, Experiment 2, the validation datasets, and the HCP dataset are shown. The frequency distribution diagrams of individual LIs for Vᴅ 1-5, and HCP data set are shown, with the pie chart showing the population proportion of lateralization preference (|LI| > 0.2).
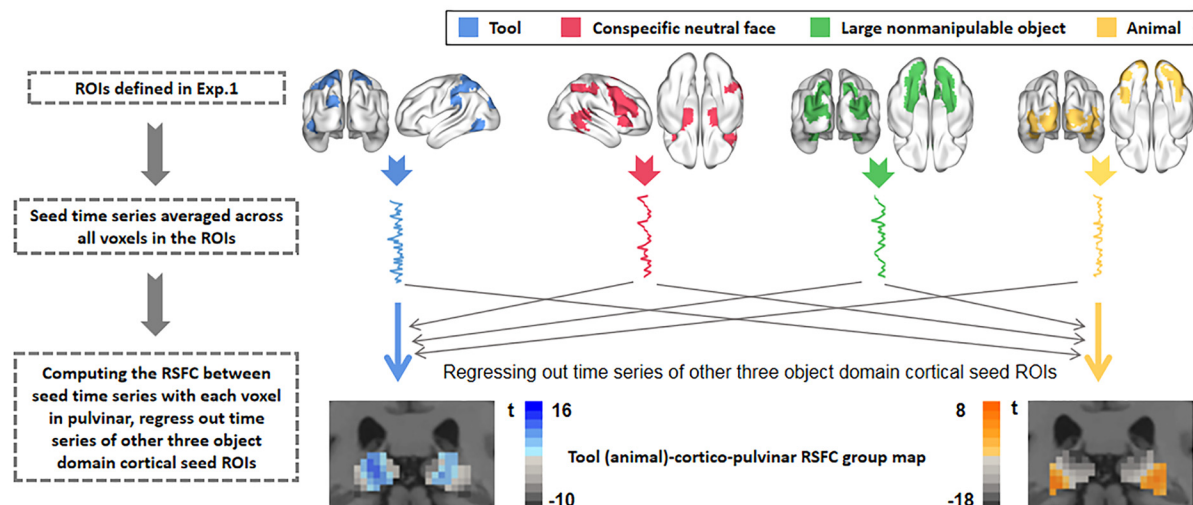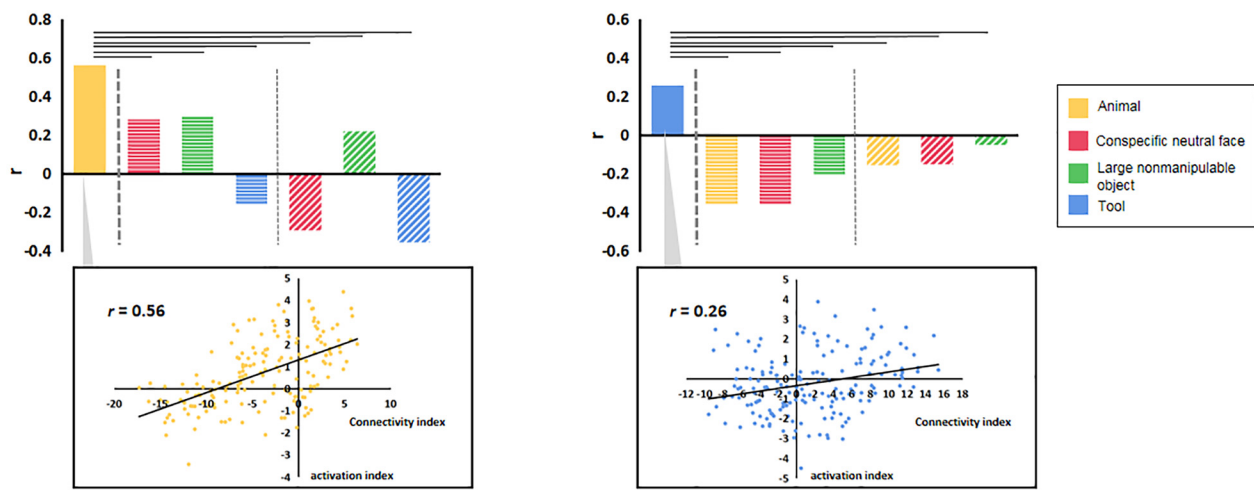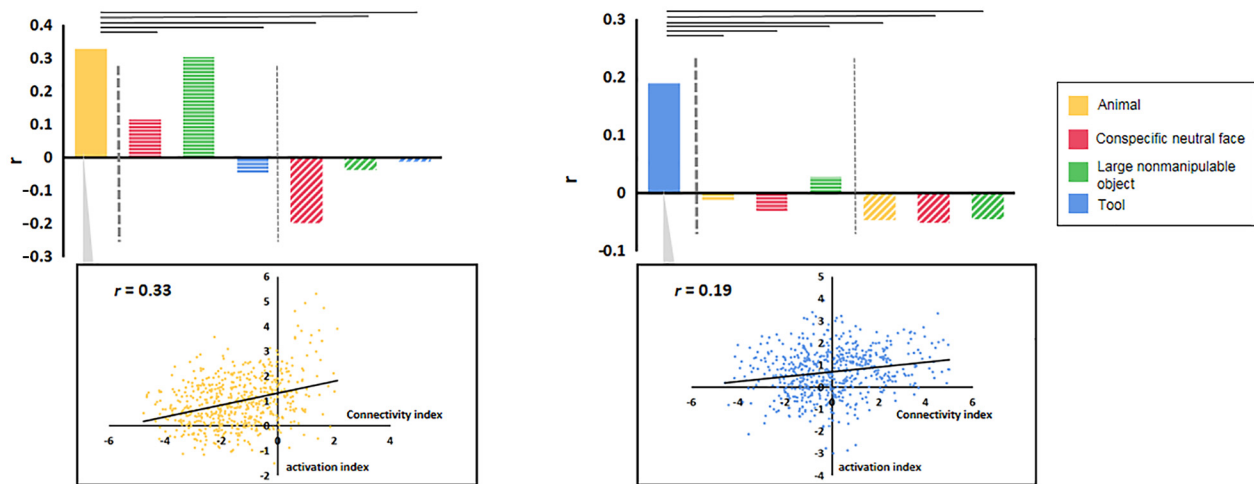
time series averaged across all voxels within each cortical seed network) and the time series of each voxel in the pulvinar, while regressing out the mean time series of the other three object domain cortical seed networks, creating a cortico-pulvinar RSFC map for each object domain (Fig. 4A; see Materials and Methods).

The r values in each pulvinar voxel of each cortico-pulvinar RSFC map reflected how strongly that voxel connected with cortical clusters showing preference for the corresponding domain. To quantify whether the pulvinar voxels' domain preference (reported in the above sections) was aligned with the their RSFC with specific object domain cortical seed network, we correlated the cortico-pulvinar RSFC maps with the pulvinar domain activation maps (t maps, each object domain vs the average of the other three object domains). As shown in Figure 4B, the within-domain correlations between the RSFC map and the domain activation map were highly significant for animals and tools (animal: $r = 0.56$, $p < 0.001$; tool: $r = 0.26$, $p < 0.001$; the left-most
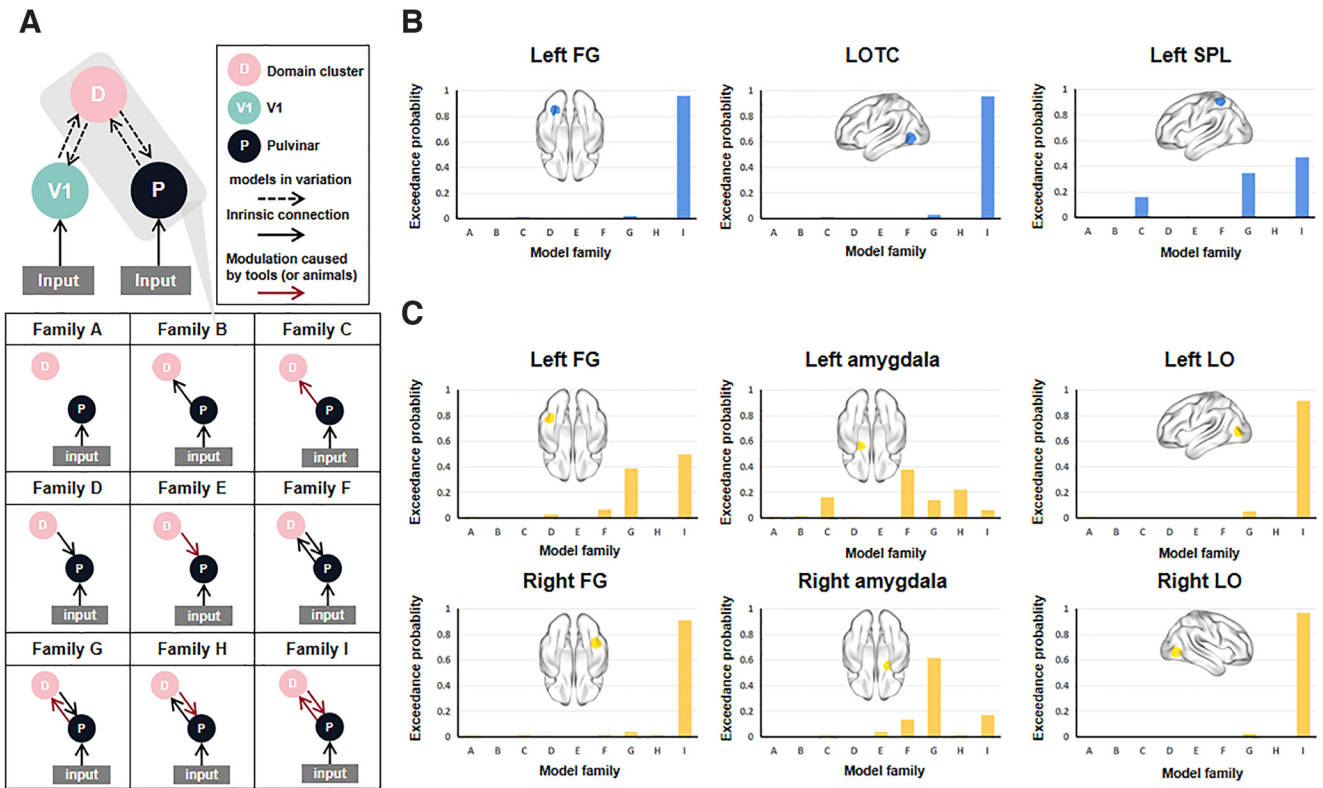
bars in each plot). That is, the more strongly a pulvinar voxel was intrinsically synchronized with animal cortical network, the more strongly it was activated by animal pictures relative to other domains, and the same pattern held for tools.

These RSFC-activation alignments were domain-specific as the cross-domain correlations were significantly lower than the within-domain correlations (Fig. 4B, shaded bars; for animals: Hotelling's t values > 3.3, Ps$_{corrected}$ < 0.01; for tools: Hotelling's t values > 3.0, Ps$_{corrected}$ < 0.05; df = 167, two-tailed, Bonferroni-corrected). The cross-domain correlations were computed by correlating the pulvinar domain activation map with RSFC-pulvinar maps with one map from the concerning interested domain (i.e., animal or tool) and the other map from the other three object domains.

Given the controversy regarding the removal of global signals in RSFC analyses, we further conducted the computation without regressing out the global signal, and the results held (for

Figure 4. The cortico-pulvinar RSFC pattern aligns with the animal and tool domain pulvinar activation patterns. **A**, Cortical ROIs for RSFC analysis and cortical-pulvinar RSFC map creation. Top, The ROIs defined for each object domain (vs the average of the other three object domains, voxel-level $p < 0.001$, one-tailed, cluster-level FWE-corrected $p < 0.05$) using Experiment 1. Bottom, A schematic overview of the cortico-pulvinar RSFC map creation. **B**, Correlations between cortico-pulvinar RSFC maps and pulvinar domain activation maps using Experiment 1 and an independent RSFC dataset ($N = 144$). Bar graphs represent correlations between animal (or tool) cortico-pulvinar RSFC map and animal (or tool) domain activation map (the leftmost bar), correlations between animal (or tool) activation map and other three object domain cortico-pulvinar RSFC maps (bars with horizontal lines), and correlations between animal (or tool) cortico-pulvinar RSFC map and other three object domain activation maps (bars with oblique lines). Solid black line indicates that Hotelling's t test between the two r values found they were significantly different ($p_{corrected} < 0.05$, df = 167, two-tailed, Bonferroni correction time = 6). Scatter plots represent the correlations between the animal (tool) cortico-pulvinar RSFC map and the pulvinar animal (tool)

Figure 5. DCM analysis results. **A**, Structure of DCM models. Top, The basic model structure. The primary visual cortex (V1), tool, or animal domain cortical (or amygdala) ROI and the pulvinar were chosen to constitute the model. The dotted arrows can be set as no connection, only intrinsic connection, and modulation caused by tools or animals. All the possible combinations of connections gave us a comprehensive model space of 80 models. Nine families were defined to partition the whole model space with no overlap, as shown in the bottom panel. **B**, Exceedance probabilities of each family for tool domain ROIs. The tool ROIs are shown in the corresponding position of the diagram. **C**, Exceedance probabilities of each family for animal domain ROIs. The animal ROIs are shown in the corresponding position of the diagram.

animals: within-domain $r = 0.58$, between-domain mean $r = -0.06$, within- vs between-domain, Hotelling's t values > 4.3, Ps$_{corrected} < 0.001$; for tools: within-domain $r = 0.29$, between-domain mean $r = -0.16$, within- vs between-domain, Hotelling's t values > 3.2, Ps$_{corrected} < 0.01$; df $= 167$). Using the HCP RSFC data preprocessed in Wen at al. (2022), the results again showed strong alignment between the RSFC pattern and the functional activation pattern in pulvinar (for animals: within-domain $r = 0.43$, between-domain mean $r = 0.03$, within- vs between-domain, Hotelling's t values > 2.9, Ps$_{corrected} < 0.05$; for tools: within-domain $r = 0.17$, between-domain mean $r = -0.09$, within- vs between-domain, Hotelling's t values > 2.8, Ps$_{corrected} < 0.05$; df $= 592$). We also tested our results with Experiment 2, where the functional activation data and the resting-state fMRI data were collected from the same group of subjects. The results showed a similar pattern (Fig. 4C).

DCM analysis results

Having established that the pulvinar has domain-differentiating response topology for tool and animal domains and that it is intrinsically connected with the corresponding domain-preferring clusters in the cortex, forming domain-specific pulvinar-cortical

←

activation map. Each dot represents a voxel in the pulvinar. **C**, Replication using Experiment 2. The ROIs were defined using Experiment 2. All object domain activation maps and object domain cortical-pulvinar RSFC maps were obtained from Experiment 2. Solid black line indicates that Hotelling's t test between the two r values found they were significantly different ($p_{corrected} < 0.05$, df $= 592$, two-tailed, Bonferroni correction time $= 6$).

networks, we next examined the direction of the information flow. We used DCM to address this question (Fig. 5A). Data from Experiment 2 were used given its relatively high spatial resolution ($2 \times 2 \times 2$ mm^3).

Model ROI definition
ROIs for the tool models and animal models included cortical regions showing tool or animal preferences, the pulvinar, and primary visual cortex. Cortical domain ROIs were obtained by drawing a sphere with an 8 mm radius centered on the peak coordinate of the domain contrast from Experiment 2 (shown in Fig. 5B,C; voxel-level $p < 0.001$, one-tailed, cluster-level FWE-corrected $p < 0.05$). Tool ROIs included the LOTC, superior parietal lobule, and FG, and we focused on the left hemisphere clusters given the strong lateralization (see above). Animal ROIs (animal vs tools and large objects) included bilateral LO and bilateral FG. We additionally included the anatomically defined bilateral amygdala (AAL template: Amygdala_L, AAL 41; Amygdala_R, AAL 42) as animal ROIs, given that it has been reported to show a preference for animals (Mormann et al., 2011; J. Yang et al., 2012) and has connections with the pulvinar (Pessoa and Adolphs, 2010). The primary visual cortex, defined as the visually activated voxels (i.e., all object domains vs rest baseline) within the Brodmann area 17, was included because of its essential role in visual processing.

Families set
The basic model structure included an object domain cortical ROI, the pulvinar, and the primary visual cortex. We considered

all possible combinations of connections (no connection, only forward connection, only backward connection, or both forward and backward connections, combined with only intrinsic connection or object domain modulation connection) between the object domain cortical ROI and the pulvinar, and between the object domain cortical ROI and the primary visual cortex, giving us a comprehensive model space of 80 models. No connection was set between the pulvinar and the primary visual cortex (McFadyen et al., 2019, 2020). We focused on information flow between the pulvinar and cortical domain-preferring clusters, defining 9 families (Fig. 5A, Family A to Family I) that partitioned the whole model space into different families with no overlap. BMS was then used to compare these competing families that represented different hypotheses.
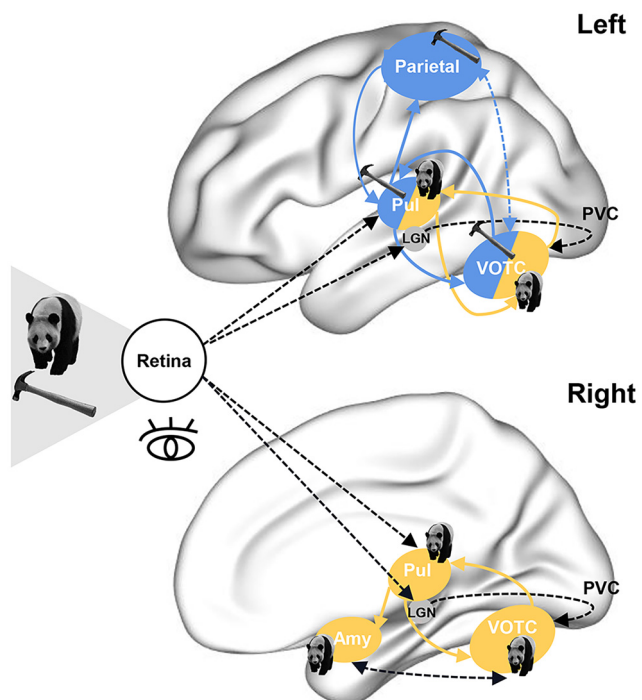
Tool results
For all the tool cortical ROIs, the best family was Family I (Fig. 5B, exceedance probability: LOTC, 0.96; left FFG, 0.96; left SPL, 0.47): bidirectional intrinsic connection and bidirectional tool-specific modulation between the pulvinar and the cortical clusters. This indicated that tool information flowed both from the pulvinar to the tool cortical clusters and from the tool cortical clusters to the pulvinar. Notably, for the left SPL, the second-best family was Family G (exceedance probability: 0.35), and the third best was Family C (exceedance probability: 0.16), which only contained forward tool modulation from the pulvinar to the SPL, indicating an essential role for forward modulation. The best model for all the tool cortical ROIs belonged to the best family, and the second and third best model for SPL also belonged to the second and third best family for SPL, respectively, which was consistent with the current best family results.

Animal results
For all the animal cortical ROIs, the best family was Family I, which contained bidirectional intrinsic connections and bidirectional animal modulations (Fig. 5C, exceedance probability: left FG, 0.50; right FG, 0.91; left LO, 0.91; right LO, 0.97), indicating the bidirectional nature of animal preference patterns in the pulvinar and cortex. For the left amygdala, the winning family was Family F (Fig. 5C, exceedance probability: 0.38), which contained only intrinsic connections between the left pulvinar and the left amygdala without any animal modulation; for the right amygdala, Family G was the winning one (Fig. 5C, exceedance probability: 0.62), which only contained animal modulation from the right pulvinar to the right amygdala. This pulvinar-amygdala right lateralization of modulation was consistent with the trend of the right lateralization observed in the local activity analyses reported above. The results using the best model were consistent with these best family results.

Discussion

Across two main experiments and multiple validation datasets (five in-house ones), we found robust, consistent tool-specific left lateralization effects in the pulvinar. Viewing pictures of tools, compared with other objects, consistently elicited stronger activation in the left pulvinar. Clusters specific to animals were also observed in the pulvinar, distributed bilaterally with a right lateralization trend. The domain selectivity strength for tools and for animals across pulvinar voxels was associated with how strongly the voxel was intrinsically connected with the cortical clusters showing the corresponding domain preference. DCM revealed that, during visual processing, the pulvinar communicated with cortical domain areas in a bidirectional fashion, with


Figure 6. Summary of pulvinar-cortical domain preference systems. The left hemisphere and right hemisphere are shown (Xia et al., 2013) in the top and bottom panels, respectively. The brain regions are shown in the approximate areas. Arrow indicates the direction of information flow. Solid line indicates the modulation found in our study. Dashed lines indicate the path found (or speculated) by previous articles. Yellow represents modulation or activation by animal images. Blue represents modulation or activation by tool images. The LGN-PVC-VOTC pathway has been described by many previous articles (e.g., Grill-Spector and Weiner, 2014). The bidirectional path between the VOTC and right amygdala was speculated by Pessoa and Adolphs (2010) and McFadyen et al. (2020). The bidirectional tool modulation between the dorsal pathway (parietal) and the ventral pathway (VOTC) was indicated by Chen et al. (2018), Garcea et al. (2019), and Lee et al. (2019). Amy, Amygdala; Pul, pulvinar; VOTC, ventral occipital temporal cortex, including lateral occipitotemporal cortex and fusiform gyrus; PVC, primary visual cortex.

modulation from the pulvinar to the superior parietal regions showing a more unique role during tool-viewing and to the right amygdala during animal-viewing (Fig. 6).

Our observation that the pulvinar contains clusters showing stronger activity to animals than other types of visual objects corresponds with findings from macaques, which observed pulvinar neurons' selectivity to threatening animate objects, such as snakes (Le et al., 2013, 2016). Interestingly, we also observed the modulation effect from the pulvinar to the right amygdala, which has also been shown to respond more strongly to animals (J. Yang et al., 2012). It has been proposed that the direct connection between pulvinar and amygdala constituted the shortcut for emotion and threatening information (Pessoa and Adolphs, 2010; McFadyen et al., 2020). In line with this proposal, animal stimuli in our experiments were indeed rated to be more threatening and of higher arousal than other objects. Thus, the pulvinar-amygdala animal-preferring pathway may support the fast fight-or-flight responses to (threatening) animals. The animal-preferring pulvinar voxels also tend to be more strongly functionally connected (bidirectional links) with cortical areas showing animal preference (e.g., bilateral FG and LO). That is, the pulvinar contains animal-preferring clusters that link with previously reported animal-preferring cortical clusters and the amygdala in a larger loop, and modulates the amygdala's response to animals, potentially serving as the gateway for animal perception.

The most robust finding of domain specificity was a preference for tool pictures in the left pulvinar. This is a highly robust left lateralization effect consistently observed across 8 datasets (i.e., two main experiments, 5 in-house validation datasets, and the HCP dataset) and across contrasts. Such left laterization of the pulvinar is aligned with cortical left lateralization effects for tools, and voxel-wise tool preference patterns in the pulvinar were associated with the intrinsic connectivity pattern with the cortical tool-preferring clusters (LOTC, SPL, and medial FG), consistent with the observation that the tool cortical regions were functionally coupled with part of the pulvinar, based on resting-fMRI analyses (Arcaro et al., 2018). Such observations provide further positive evidence of the pulvinar's role in giving rise to tool selectivity, which has been speculated based on indirect evidence (Fang and He, 2005; Wilke et al., 2018). While the DCM results supported bidirectional connections among these regions, it is worth noting that the model with modulation only from the pulvinar to the parietal clusters also had a higher exceedance probability. That is, tool selectivity in the left pulvinar might be more than mere peripheral feedback activation from left-lateralized tool cortical network but rather an integral constituent of a left-lateralized cortical-subcortical network for tool processing.

The origin and functionality of lateralization in the human brain are controversial, with some proposing that lateralization increases processing efficiency (Rogers et al., 2004; Vallortigara, 2006; Corballis, 2017). Regarding tools, the left brain lateralization is observed in humans and often discussed relating to the right-handedness (e.g., Lewis, 2006). Intriguingly, Cheng et al. (2021) examined white matter structural connectivity patterns across species and showed that macaques and humans differed significantly in the lateralization effect in the IPL, a region that has been consistently implicated in tool processing in humans. Humans showed leftward asymmetric connectivity between the IPL and regions, including the primary motor cortex, ventral premotor cortex, SPL, and posterior MTG, but macaques showed no significant leftward asymmetric connections. Our present results showed that such left hemispheric advantage for tools is not only a cortical signature but also robustly manifested in subcortical structures; relationship between such tentative human-specific brain patterns for tools and human-specific complex tool use behavior (Gibson et al., 1994; Vaesen, 2012) requires further investigation.

More generally, how do the observations of pulvinar response and connectivity patterns contribute to theories about visual object processing in the brain? What information about tools and animals is being processed in the pulvinar? Traditional object domain processing theory primarily focuses on cortical processing, where low-level, retinotopic visual information processed in V1 is organized into higher-level visual and nonvisual representations downstream that give rise to the animacy domain structure observed later on, without explicit assumptions about the functionality of subcortical structures (e.g., Grill-Spector and Weiner, 2014). A related proposal emphasizes that the domain structure also partly reflects an organization that is driven by the perception-response loop, the way that the brain processes sensory signals is constrained by how optimally they map onto responses for survival (Mahon and Caramazza, 2011; Peelen and Downing, 2017; Bi, 2020; Fan et al., 2021). This notion predicts that the evolutionarily salient domain structures cut across all stages of the perception-response system, even in subcortical structures, manifested along with the intrinsic properties of each stage. In our experiments on the pulvinar, we matched different domains of images on low-level

visual image properties, including mean luminance, contrast, color (all grayscale images), and spatial frequency; thus, the pulvinar selectivity patterns were not simply driven by such information. Nonetheless, animal and tool pictures still tend to differ along other higher-level visual information, such as shape, size, and texture, with tools being more elongated in shape, having smaller (real-world) size, smoother, aligning with the existing literature (Konkle and Caramazza, 2013; Chen et al., 2018; Long et al., 2018). These sensory signals are also differently associated with many other types of nonvisual information that varies across domains, including the types of responses, such as fight-or-flight (for animals) and grasping, manipulation, and functional use (for tools). Whether the object domain effects observed in the cortical regions are reducible to some specific or combinations of these properties are still under debate (e.g., Grill-Spector and Weiner, 2014; Nasr et al., 2014; Bryan et al., 2016; Fabbri et al., 2016; Proklova et al., 2016; Bracci et al., 2019; Yue et al., 2020; Fan et al., 2021). Along the same line, what exactly pulvinar processes to give rise to the observed domain sensitivity and connectivity patterns, and potentially other subcortical structures, such as LGN and SC, remain to be vigorously tested with specific hypotheses and finer measurements.

A few open issues need to be considered. Arcaro et al. (2018) reported face preferences in the medial pulvinar. While we also observed such an effect in Experiment 1, we only found right lateralization of face preferences without any voxels surviving correction in Experiment 2. Compared with the other object categories, the face category comprises items of greater homogeneity (subordinates), which may introduce stronger repetition suppression effects. The robustness of the face effects in pulvinar thus remain to be further examined. Second, for the DCM analysis, we did not test the fully possible range of connections among all regions (cortical and subcortical) but focused on the information flow between the pulvinar and other regions. Choosing all regions and connections at a time may give a more comprehensive understanding, but also results in a huge computational burden and make the model too complex. Finally, we only examined the (resting-state and task) functional connectivity of pulvinar in the current study and did not have structural connectivity data on the same subjects. The relationship between structural and functional connectivity is a general question of the brain research (e.g., see discussions in Honey et al., 2009). The few studies on pulvinar have reported general alignment: Arcaro et al. (2015) reported, in both RSFC and diffusion-weighted imaging data, the ventral pulvinar were more strongly connected with early and associative visual cortex whereas the dorsal pulvinar with frontoparietal regions. McFadyen et al. (2019) reported a subcortical structural pathway from superior colliculus via pulvinar to amygdala underlying the recognition of fearful faces. The more comprehensive structural subcortical-cortical pathway underlying the functional domain network remain to be further charted, and the current functional connectivity results guide such investigations.

In conclusion, we have shown that visual processing of different domains of objects (animals and tools) triggers different patterns of response in the pulvinar, with robust left lateralization for tool pictures and distinct, bilateral (rightward) clusters for animals, which aligns with domain-specific cortical (and amygdala) activation patterns through intrinsic and task-based functional connectivity. While the pulvinar and cortical domain-specific clusters overall show bidirectionality, the pulvinar-to-right-amygdala path shows a one-way shortcut supporting the perception of animals; the modulation connection from the pulvinar to superior parietal

cortex shows an advantage in the perception of tools. These results incorporate subcortical regions, especially the pulvinar, into the object processing network and highlight the need for coherent visual theories that explain the mechanisms underlying domain-appearing-organization across various processing stages.

References

Arcaro MJ, Pinsk MA, Kastner S (2015) The anatomical and functional organization of the human visual pulvinar. J Neurosci 35:9848–9871.

Arcaro MJ, Pinsk MA, Chen J, Kastner S (2018) Organizing principles of pulvino-cortical functional coupling in humans. Nat Commun 9:5382.

Arshad Q, Nigmatullina Y, Bronstein AM (2013) Handedness-related cortical modulation of the vestibular-ocular reflex. J Neurosci 33:3221–3227.

Ashburner J (2007) A fast diffeomorphic image registration algorithm. Neuroimage 38:95–113.

Bai L, Hui M, Yu-Xia H (2005) The development of native Chinese affective picture system: a pretest in 46 college students. Chin Ment Health J 19:719–722.

Barch DM, et al. WU-Minn HCP Consortium (2013) Function in the human connectome: task-fMRI and individual differences in behavior. Neuroimage 80:169–189.

Baumgartner E, Gegenfurtner KR (2016) Image statistics and the representation of material properties in the visual cortex. Front Psychol 7:1185.

Benevento LA, Miller J (1981) Visual responses of single neurons in the caudal lateral pulvinar of the macaque monkey. J Neurosci 1:1268–1278.

Bi Y (2020) Concepts and object domains. In: The cognitive neurosciences (Poeppel D, Mangun GR, Gazzaniga MS, eds). Cambridge, MA: Massachusetts Institute of Technology.

Bi Y, Wang X, Caramazza A (2016) Object domain and modality in the ventral visual pathway. Trends Cogn Sci 20:282–290.

Bracci S, Ritchie JB, Kalfas I, Op de Beeck HP (2019) The ventral visual pathway represents animal appearance over animacy, unlike human behavior and deep neural networks. J Neurosci 39:6513–6525.

Brandi ML, Wohlschlager A, Sorg C, Hermsdorfer J (2014) The neural correlates of planning and executing actual tool use. J Neurosci 34:13183–13194.

Bridge H, Leopold DA, Bourne JA (2016) Adaptive pulvinar circuitry supports visual cognition. Trends Cogn Sci 20:146–157.

Bryan PB, Julian JB, Epstein RA (2016) Rectilinear edge selectivity is insufficient to explain the category selectivity of the parahippocampal place area. Front Hum Neurosci 10:137.

Chen J, Snow JC, Culham JC, Goodale MA (2018) What role does 'elongation' play in 'tool-specific' activation and connectivity in the dorsal and ventral visual streams? Cereb Cortex 28:1117–1131.

Cheng L, Zhang Y, Li G, Wang J, Sherwood C, Gong G, Fan L, Jiang T (2021) Connectional asymmetry of the inferior parietal lobule shapes hemispheric specialization in humans, chimpanzees, and rhesus macaques. Elife 10:e67600.

Cohen J (1960) A coefficient of agreement for nominal scales. Educ Psychol Meas 20:37–46.

Corballis MC (2017) The evolution of lateralized brain circuits. Front Psychol 8:1021.

Fabbri S, Stubbs KM, Cusack R, Culham JC (2016) Disentangling representations of object and grasp properties in the human brain. J Neurosci 36:7648–7662.

Fan S, Wang X, Wang X, Wei T, Bi Y (2021) Topography of visual features in the human ventral visual pathway. Neurosci Bull 37:1454–1468.

Fang F, He S (2005) Cortical responses to invisible objects in the human dorsal and ventral pathways. Nat Neurosci 8:1380–1385.

Fiebelkorn IC, Kastner S (2019) The puzzling pulvinar. Neuron 101:201–203.

Friston KJ, Williams S, Howard R, Frackowiak RS, Turner R (1996) Movement-related effects in fMRI time-series: movement artifacts in fMRI. Magn Reson Med 35:346–355.

Friston KJ, Harrison L, Penny W (2003) Dynamic causal modelling. Neuroimage 19:1273–1302.

Garcea FE, Almeida J, Sims MH, Nunno A, Meyers SP, Li YM, Walter K, Pilcher WH, Mahon BZ (2019) Domain-specific diaschisis: lesions to parietal action areas modulate neural responses to tools in the ventral stream. Cereb Cortex 29:3168–3181.

Garcea FE, Buxbaum LJ (2019) Gesturing tool use and tool transport actions modulates inferior parietal functional connectivity with the dorsal and ventral object processing pathways. Hum Brain Mapp 40:2867–2883.

Gibson KR, Gibson KR, Ingold T (1994) Tools, language and cognition in human evolution. Cambridge: Cambridge UP.

Glasser MF, Sotiropoulos SN, Wilson JA, Coalson TS, Fischl B, Andersson JL, Xu J, Jbabdi S, Webster M, Polimeni JR, Van Essen DC, Jenkinson M, WU-Minn HCP Consortium (2013) The minimal preprocessing pipelines for the Human Connectome Project. Neuroimage 80:105–124.

Grill-Spector K, Weiner KS (2014) The functional architecture of the ventral temporal cortex and its role in categorization. Nat Rev Neurosci 15:536–548.

Guedj C, Vuilleumier P (2020) Functional connectivity fingerprints of the human pulvinar: decoding its role in cognition. Neuroimage 221:117162.

He C, Peelen MV, Han Z, Lin N, Caramazza A, Bi Y (2013) Selectivity for large nonmanipulable objects in scene-selective visual cortex does not require visual experience. Neuroimage 79:1–9.

Honey CJ, Sporns O, Cammoun L, Gigandet X, Thiran JP, Meuli R, Hagmann P (2009) Predicting human resting-state functional correlation from structural correlation. Proc Natl Acad Sci USA 106:2035–2040.

Jaramillo J, Mejias JF, Wang XJ (2019) Engagement of pulvino-cortical feed-forward and feedback pathways in cognitive computations. Neuron 101:321–336.e5.

Koizumi A, Zhan M, Ban H, Kida I, De Martino F, Vaessen MJ, de Gelder B, Amano K (2019) Threat anticipation in pulvinar and in superficial layers of primary visual cortex (V1): evidence from layer-specific ultra-high field 7T fMRI. eNeuro 6:ENEURO.0429-19.2019.

Konkle T, Caramazza A (2013) Tripartite organization of the ventral stream by animacy and object size. J Neurosci 33:10235–10242.

Krauth A, Blanc R, Poveda A, Jeanmonod D, Morel A, Székely G (2010) A mean three-dimensional atlas of the human thalamus: generation from multiple histological data. Neuroimage 49:2053–2062.

Le QV, Isbell LA, Matsumoto J, Nguyen M, Hori E, Maior RS, Tomaz C, Tran AH, Ono T, Nishijo H (2013) Pulvinar neurons reveal neurobiological evidence of past selection for rapid detection of snakes. Proc Natl Acad Sci USA 110:19000–19005.

Le QV, Isbell LA, Matsumoto J, Le VQ, Nishimaru H, Hori E, Maior RS, Tomaz C, Ono T, Nishijo H (2016) Snakes elicit earlier, and monkey faces, later, gamma oscillations in macaque pulvinar neurons. Sci Rep 6:20595.

Lee D, Mahon BZ, Almeida J (2019) Action at a distance on object-related ventral temporal representations. Cortex 117:157–167.

Lewis JW (2006) Cortical networks related to human use of tools. Neuroscientist 12:211–231.

Liu TT, Nalci A, Falahpour M (2017) The global signal in fMRI: nuisance or information? Neuroimage 150:213–229.

Long B, Yu CP, Konkle T (2018) Mid-level visual features underlie the high-level categorical organization of the ventral stream. Proc Natl Acad Sci USA 115:E9015–E9024.

Mahon BZ, Caramazza A (2011) What drives the organization of object knowledge in the brain? Trends Cogn Sci 15:97–103.

Maldjian JA, Laurienti PJ, Kraft RA, Burdette JH (2003) An automated method for neuroanatomic and cytoarchitectonic atlas-based interrogation of fMRI data sets. Neuroimage 19:1233–1239.

Mattioni S, Rezk M, Battal C, Bottini R, Cuculiza Mendoza KE, Oosterhof NN, Collignon O (2020) Categorical representation from sound and sight in the ventral occipito-temporal cortex of sighted and blind. Elife 9:e50732.

McFadyen J, Mermillod M, Mattingley JB, Halász V, Garrido MI (2017) A rapid subcortical amygdala route for faces irrespective of spatial frequency and emotion. J Neurosci 37:3864–3874.

McFadyen J, Mattingley JB, Garrido MI (2019) An afferent white matter pathway from the pulvinar to the amygdala facilitates fear recognition. Elife 8:e40766.

McFadyen J, Dolan RJ, Garrido MI (2020) The influence of subcortical short-cuts on disordered sensory and cognitive processing. Nat Rev Neurosci 21:264–276.

Mormann F, Dubois J, Kornblith S, Milosavljevic M, Cerf M, Ison M, Tsuchiya N, Kraskov A, Quiroga RQ, Adolphs R, Fried I, Koch C (2011) A category-specific response to animals in the right human amygdala. Nat Neurosci 14:1247–1249.

Murphy K, Fox MD (2017) Towards a consensus regarding global signal regression for resting state functional connectivity MRI. Neuroimage 154:169–173.

Nasr S, Echavarria CE, Tootell RB (2014) Thinking outside the box: rectilinear shapes selectively activate scene-selective cortex. J Neurosci 34:6721–6735.

Nguyen MN, Nishimaru H, Matsumoto J, Van Le Q, Hori E, Maior RS, Tomaz C, Ono T, Nishijo H (2016) Population coding of facial information in the monkey superior colliculus and pulvinar. Front Neurosci 10:583.

Öhman A (2005) The role of the amygdala in human fear: automatic detection of threat. Psychoneuroendocrinology 30:953–958.

Peelen MV, Downing PE (2017) Category selectivity in human visual cortex: beyond visual object recognition. Neuropsychologia 105:177–183.

Penny WD, Stephan KE, Daunizeau J, Rosa MJ, Friston KJ, Schofield TM, Leff AP (2010) Comparing families of dynamic causal models. PLoS Comput Biol 6:e1000709.

Pessoa L, Adolphs R (2010) Emotion processing and the amygdala: from a 'low road' to 'many roads' of evaluating biological significance. Nat Rev Neurosci 11:773–783.

Proklova D, Kaiser D, Peelen MV (2016) Disentangling representations of object shape and object category in human visual cortex: the animate–inanimate distinction. J Cogn Neurosci 28:680–692.

Rogers LJ, Zucca P, Vallortigara G (2004) Advantages of having a lateralized brain. Proc R Soc Lond B Biol Sci 271:S420–S422.

Saalmann YB, Kastner S (2011) Cognitive and perceptual functions of the visual thalamus. Neuron 71:209–223.

Schone HR, Maimon-Mor RO, Baker CI, Makin TR (2021) Expert tool users show increased differentiation between visual representations of hands and tools. J Neurosci 41:2980–2989.

Seghier ML (2008) Laterality index in functional MRI: methodological issues. Magn Reson Imaging 26:594–601.

Song XW, Dong ZY, Long XY, Li SF, Zuo XN, Zhu CZ, He Y, Yan CG, Zang YF (2011) REST: a toolkit for resting-state functional magnetic resonance imaging data processing. PLoS One 6:e25031.

Stephan KE, Penny WD, Moran RJ, den Ouden HE, Daunizeau J, Friston KJ (2010) Ten simple rules for dynamic causal modeling. Neuroimage 49:3099–3109.

Striem-Amit E, Vannuscorps G, Caramazza A (2018) Plasticity based on compensatory effector use in the association but not primary sensorimotor cortex of people born without hands. Proc Natl Acad Sci USA 115:7801–7806.

Szaflarski JP, Holland SK, Schmithorst VJ, Byars AW (2006) fMRI study of language lateralization in children and adults. Hum Brain Mapp 27:202–212.

Tzourio-Mazoyer N, Landeau B, Papathanassiou D, Crivello F, Etard O, Delcroix N, Mazoyer B, Joliot M (2002) Automated anatomical labeling of activations in SPM using a macroscopic anatomical parcellation of the MNI MRI single-subject brain. Neuroimage 15:273–289.

Vaesen K (2012) The cognitive bases of human tool use. Behav Brain Sci 35:203–218.

Vallortigara G (2006) The evolutionary psychology of left and right: costs and benefits of lateralization. Dev Psychobiol 48:418–427.

van den Hurk J, Van Baelen M, Op de Beeck HP (2017) Development of visual category selectivity in ventral visual cortex does not require visual experience. Proc Natl Acad Sci 114:E4501–E4510.

Van Essen DC, Smith SM, Barch DM, Behrens TE, Yacoub E, Ugurbil K, WU-Minn HCP Consortium (2013) The WU-Minn Human Connectome Project: an overview. Neuroimage 80:62–79.

Wang X, Fang Y, Cui Z, Xu Y, He Y, Guo Q, Bi Y (2016) Representing object categories by connections: evidence from a mutivariate connectivity pattern classification approach. Decoding object categories via fcMVPA. Hum Brain Mapp 37:3685–3697.

Wang X, He C, Peelen MV, Zhong S, Gong G, Caramazza A, Bi Y (2017) Domain selectivity in the parahippocampal gyrus is predicted by the same structural connectivity patterns in blind and sighted individuals. J Neurosci 37:4705–4716.

Wang X, Zhuang T, Shen J, Bi Y (2018) Disentangling representations of shape and action components in the tool network. Neuropsychologia 117:199–210.

Ward R, Calder AJ, Parker M, Arend I (2007) Emotion recognition following human pulvinar damage. Neuropsychologia 45:1973–1978.

Wen H, Xu T, Wang X, Yu X, Bi Y (2022) Brain intrinsic connection patterns underlying tool processing in human adults are present in neonates and not in macaques. Neuroimage 258:119339.

Wilke M, Lidzba K (2007) LI-tool: a new toolbox to assess lateralization in functional MR-data. J Neurosci Methods 163:128–136.

Wilke M, Schneider L, Dominguez-Vargas AU, Schmidt-Samoa C, Miloserdov K, Nazzal A, Dechent P, Cabral-Calderin Y, Scherberger H, Kagan I, Bähr M (2018) Reach and grasp deficits following damage to the dorsal pulvinar. Cortex 99:135–149.

Willenbockel V, Sadr J, Fiset D, Horne GO, Gosselin F, Tanaka JW (2010) Controlling low-level image properties: the SHINE toolbox. Behav Res Methods 42:671–684.

Wu W, Wang X, Wei T, He C, Bi Y (2020) Object parsing in the left lateral occipitotemporal cortex: whole shape, part shape, and graspability. Neuropsychologia 138:107340.

Xia M, Wang J, He Y (2013) BrainNet Viewer: a network visualization tool for human brain connectomics. PLoS One 8:e68910.

Yan CG, Wang XD, Zuo XN, Zang YF (2016) DPABI: data processing and analysis for (resting-state) brain imaging. Neuroinformatics 14:339–351.

Yang H, Lin Q, Han Z, Li H, Song L, Chen L, He Y, Bi Y (2017) Dissociable intrinsic functional networks support noun-object and verb-action processing. Brain Lang 175:29–41.

Yang J, Bellgowan PS, Martin A (2012) Threat, domain-specificity and the human amygdala. Neuropsychologia 50:2566–2572.

Yue X, Robert S, Ungerleider LG (2020) Curvature processing in human visual cortical areas. Neuroimage 222:117295.

Zachariou V, Del Giacco AC, Ungerleider LG, Yue X (2018) Bottom-up processing of curvilinear visual features is sufficient for animate/inanimate object categorization. J Vis 18:3.

Zeidman P, Jafarian A, Corbin N, Seghier ML, Razi A, Price CJ, Friston KJ (2019a) A guide to group effective connectivity analysis: 1. First level analysis with DCM for fMRI. Neuroimage 200:174–190.

Zeidman P, Jafarian A, Seghier ML, Litvak V, Cagnan H, Price CJ, Friston KJ (2019b) A guide to group effective connectivity analysis: 2. Second level analysis with PEB. Neuroimage 200:12–25.